GLIA

WILEY

RESEARCH ARTICLE

Cannabinoid receptor 2 is necessary to induce toll-like receptor-mediated microglial activation

Nico Reusch[1,2] | Kishore Aravind Ravichandran[3] | Bolanle Fatimat Olabiyi[3] |
Joanna Agnieszka Komorowska-Müller[3,4] | Jan N. Hansen[5] | Thomas Ulas[1,2,6] |
Marc Beyer[6,7] | Andreas Zimmer[3] | Anne-Caroline Schmöle[3]

[1]Systems Medicine, German Center for Neurodegenerative Diseases (DZNE), Bonn, Germany

[2]Genomics and Immunoregulation, Life and Medical Sciences Institute (LIMES), Bonn, Germany

[3]Institute for Molecular Psychiatry, Medical Faculty, University of Bonn, Bonn, Germany

[4]International Max Planck Research School for Brain and Behavior, University of Bonn, Bonn, Germany

[5]Institute of Innate Immunity, Biophysical Imaging, Medical Faculty, University of Bonn, Bonn, Germany

[6]Platform for Single Cell Genomics and Epigenomics (PRECISE), German Center for Neurodegenerative Diseases (DZNE), University of Bonn, Bonn, Germany

[7]Molecular Immunology in Neurodegeneration, German Center for Neurodegenerative Diseases (DZNE), Bonn, Germany

Correspondence
Anne-Caroline Schmöle, Institute for Molecular Psychiatry, Medical Faculty, University of Bonn, Venusberg-Campus 1, Bonn 53127, Germany.
Email: anne.schmoele@uni-bonn.de

Abstract

The tight regulation of microglia activity is key for precise responses to potential threats, while uncontrolled and exacerbated microglial activity is neurotoxic. Microglial toll-like receptors (TLRs) are indispensable for sensing different types of assaults and triggering an innate immune response. Cannabinoid receptor 2 (CB2) signaling is a key pathway to control microglial homeostasis and activation, and its activation is connected to changes in microglial activity. We aimed to investigate how CB2 signaling impacts TLR-mediated microglial activation. Here, we demonstrate that deletion of CB2 causes a dampened transcriptional response to prototypic TLR ligands in microglia. Loss of CB2 results in distinct microglial gene expression profiles, morphology, and activation. We show that the CB2-mediated attenuation of TLR-induced microglial activation is mainly p38 MAPK-dependent. Taken together, we demonstrate that CB2 expression and signaling are necessary to fine-tune TLR-induced activation programs in microglia.

KEYWORDS
cannabinoid receptor 2 (CB2), endocannabinoid system, microglia, neuroinflammation, RNA sequencing

---

Nico Reusch and Kishore Aravind Ravichandran contributed equally to this study.

---

1 | INTRODUCTION

Neuroinflammation is a crucial process that precedes or accompanies a variety of neurodegenerative diseases. It is characterized by the release of cytokines, reactive oxygen species, and growth factors with neurotoxic effects. Microglia are the resident immune cells of the brain and therefore one of the key players in neuroinflammation (Wolf, Boddeke, & Kettenmann, 2017). Consequently, it is of great importance to understand, on the one hand, how microglia contribute to neuroinflammatory processes and, on the other hand, how microglial activity can be controlled.

The innate immune system triggers an inflammatory cascade by binding of pathogen-associated molecular patterns (PAMPs) to pattern-recognition receptors (PRR). Toll-like receptors (TLR) belong to this receptor family and induce an intracellular signaling cascade leading to the production of different cytokines and especially chemokines (Kawasaki & Kawai, 2014). TLR ligands include viral double-stranded RNA (TLR3), bacterial lipopolysaccharide (LPS) (TLR4) or unmethylated CpG DNA (TLR9). TLRs are located either on the cell surface (such as TLR4) or within endosomes (including TLR3 and TLR9) and can initiate different downstream signaling cascades. All TLRs besides TLR3 activate myeloid differentiation primary response gene 88 (MyD88)-dependent signaling, whereas TLR3 uses TIR-domain-containing adapter-inducing interferon-β (TRIF) as its sole adapter. Furthermore, TLR4 signaling acts on both MyD88- and TRIF-related adapter molecules (TRAM) (Kielian, 2006). Through a number of accessory molecules and transcription factors, activation of TLRs results in the expression of pro-inflammatory cytokines and interferon (IFN)-inducible genes (Akira & Takeda, 2004), initially observed in peripheral immune cells but also described for microglia in recent years (Fiebich, Batista, Saliba, Yousif, & de Oliveira, 2018).

The endocannabinoid system (ECS) encompasses the G-protein coupled receptors CB1 and CB2 as well as endogenous ligands and enzymes for biosynthesis, transport and degradation. Downstream signaling is mediated via mitogen-activated protein kinase (MAPK) signaling with extracellular signal-regulated kinases (ERK) as key molecule (Ibsen, Connor, & Glass, 2017). The cannabinoid receptor (CB) 1 (CB1) is predominantly expressed on neurons, whereas the CB2 receptor is primarily located on peripheral immune cells (Pacher & Mechoulam, 2011). Under healthy conditions, CB2 is weakly expressed in the brain and is mainly found in microglia cells (Schmöle et al., 2015). In addition, low expression of CB2 could also be detected on neurons, where its activation regulates neuronal excitability (Stempel et al., 2014). Under inflammatory conditions, CB2 expression is upregulated on microglia and can also be expressed by T cells, macrophages or astrocytes. However, expression levels depend on the inflammatory context (Benito et al., 2008). Treatment of microglia with CB2 agonists reduced the pro-inflammatory response after challenge with LPS or IFN-γ (Ehrhart et al., 2005; Ma et al., 2015). Subsequently, stimulation with the CB2 agonists 2-arachidonylglycerol (2-AG) and anandamide induced an anti-inflammatory phenotype in microglia (Mecha et al., 2015). Overall, these observations support a model where CB2 activation promotes a shift from pro-inflammatory microglial activation to an anti-inflammatory phenotype (Tanaka, Sackett, & Zhang, 2020) thus dampening the inflammatory response.

The interaction of the ECS with TLRs is not well understood. It was shown that TLR-mediated inflammation can influence CB2 expression, but also that CB2 activity manipulates inflammatory responses. Yet, the underlying mechanisms for both observations remain elusive. It has been reported that endocannabinoids suppress LPS-induced production of pro-inflammatory mediators such as NO or interleukin-1β (IL-1β) by monocytes, microglia or macrophages in vitro (Ma et al., 2015; Mestre et al., 2005; Molina-Holgado et al., 2003; Zheng & Specter, 1996; Zurier, Rossetti, Burstein, & Bidinger, 2003). In line with this, treatment of mice with cannabinoids or synthetic CB2 agonists leads to a decreased production of inflammatory cytokines and limited infiltration of neutrophils resulting in an increased survival of mice after LPS injection (Berdyshev, Boichot, Corbel, Germain, & Lagente, 2002; Gallily et al., 1997; Roche, Diamond, Kelly, & Finn, 2006; Smith, Terminelli, & Denhardt, 2000). In contrast, mice lacking the CB2 receptor show enhanced IL-6 production and tissue damage in a sepsis model (Tschöp et al., 2009). Finally, murine monocytes treated with LPS or IFN-γ in vivo or in vitro show enhanced CB2 expression (Concannon, Okine, Finn, & Dowd, 2015; Maresz, Carrier, Ponomarev, Hillard, & Dittel, 2005; Mukhopadhyay et al., 2006). However, studies focusing on the interaction of CB2 with TLR4, other TLRs besides TLR4 are lacking. E.g. interaction of TLR3 with the ECS has only been studied indirectly as the role of the cannabinoid anandamide-degrading enzyme fatty acid amide hydrolase (FAAH) (Flannery, Henry, Kerr, Finn, & Roche, 2018; Henry, Kerr, Finn, & Roche, 2014) was investigated in context of TLR3 signaling while the role of CB2 was not directly studied.

We have previously reported that microglia from mice lacking the CB2 receptor show a reduced inflammatory phenotype after in vitro stimulation with LPS/IFN-γ or in vivo in a mouse model of Alzheimer's Disease (AD) (Schmöle et al., 2015, 2018), whereas the underlying molecular mechanisms remained unclear. In particular the striking differences in the response of CB2 knockout (CB2$^{-/-}$) and wildtype (WT) microglia to LPS/IFN-γ stimulation suggested a potential role for CB2 in the orchestration and attenuation of TLR-mediated microglial activation and warrant to study the underlying mechanism in more detail. Thus, we aimed to characterize the inflammatory profile of CB2$^{-/-}$ microglia in response to different TLR stimulations and investigate the molecular targets that connect CB2 signaling to TLR-mediated microglial activation.

Here we performed a systematic characterization of the transcriptional, morphological and secretory changes induced by TLR-mediated activation of microglia from CB2$^{-/-}$ mice. We stimulated primary microglia from WT and CB2$^{-/-}$ mice with ligands for TLR3 (polyinosinic-polycytidylic acid [PolyI:C]), TLR4 (LPS/IFN-γ) and TLR9 (CpG). We demonstrate that stimulation of CB2$^{-/-}$ microglia with all three TLR ligands results in a dampened inflammatory gene expression profile. Furthermore, phenotypic microglial activation is significantly reduced in CB2$^{-/-}$ mice after all three stimulations, suggesting that the presence of the CB2 receptor is necessary to induce the full TLR-mediated microglial activation program. Finally, we identified p38

MAPK signaling as a potential mechanism that connects CB2 signaling with TLR-mediated microglial activation.

2 | MATERIAL AND METHODS

2.1 | Microglia cultures

Primary neonatal microglia were generated from 1 to 5 days old C57BL/6J (WT) and B6.Cg-Cnr2tm1Zim (CB2$^{-/-}$) pups (Buckley et al., 2000). C57BL/6J were originally obtained from a commercial breeder (Charles River) and bred in house. CB2$^{-/-}$ mice were bred homozygous and backcrossed to the C57BL/6J line every six generations to minimize the risk of genetic drift.

Briefly, after decapitation, extracted brains were collected in ice-cold PBS. Cortices of both hemispheres were collected after removal of meninges and triturated until a single-cell suspension was achieved. Isolated cells were cultivated as mixed glia culture until they reached confluency after approximately 14 days. Cells were cultivated in DMEM high glucose (Gibco, Darmstadt, Germany) containing 10% fetal calf serum (FCS) (PAA, Freiburg, Germany), 1% penicillin/ streptomycin (Gibco). The medium was changed twice weekly. Microglia cells were harvested by shaking for 1 h at 200 rpm and re-seeded in 24-well plates for stimulation experiments at a density of 1.5×10^5 cells/ml. After re-seeding, cells were rested for 24 h.

For stimulation experiments, cells were treated for 30 min or 16 h with *Escherichia coli* LPS serotype 0127:B8 (100 ng/ml) (Sigma-Aldrich, Taufkirchen, Germany) and IFN-γ (20 ng/ml) (R&D Systems, Wiesbaden, Germany), CpG (1 nmol/ml), or PolyI:C (50 μg/ml).

2.2 | Organotypic hippocampal slice cultures

Organotypic hippocampal slice cultures (OHSCs) were prepared from 4 to 6 days old WT and CB2$^{-/-}$ pups. Mice were decapitated and extracted brains were transferred into ice-cold dissection medium (Modified Eagle medium (MEM) with 1% HEPES, 1% Glutamine and 1% penicillin/streptomycin (all from Gibco). The cerebellum was removed, and 2–4 brains were dorsally super-glued to the vibratome platform supported by 2% agarose block. The brains were immersed in dissection medium in the vibratome and were horizontally sectioned into 350 μm thick slices. The sectioned slices were quickly transferred into culture dishes containing ice-cold dissection medium. The intact hippocampal regions CA1, CA2, CA3, dentate gyrus, and the entorhinal cortex, were dissected and transferred into new culture dishes. The hippocampal slices were then placed on translucent semi-porous membrane (Millipore CM cell culture inserts) (2 slices/insert) and were transferred to six-well plates filled with 1 ml culture medium (MEM supplemented with 25% Hank's balanced salt solution (HBSS), 25% heat-inactivated FCS, 1% Glutamine, 1% penicillin/streptomycin (all Gibco), 1% Amphotericin-B and 4.5% D-Glucose (both Sigma). The OHSCs were cultured at 37°C and 5% CO$_2$ for 14 days. The culture medium was changed every other day.

For stimulation experiments, OHSCs were treated for 16 h with LPS (100 ng/ml) and IFN-γ (20 ng/ml), CpG (1 nmol/ml), or PolyI:C (50 μg/ml).

2.3 | Bone-marrow derived macrophages

Bone-marrow (BM) cells for generation of macrophages were isolated from the hindleg of mice and were cultured in 1.5×10^5 cells/ml in RPMI supplemented with 10% (vol/vol) heat-inactivated FCS, 1% glutamine, 1% penicillin/streptomycin, 0.1% β-mercaptoethanol (all from Gibco), and 15% conditioned medium of L929 cells. On day 3, medium was changed, and adherent cells were harvested on day 6. For stimulation experiments, BM-derived macrophages were treated for 16 h with LPS (100 ng/ml) and IFN-γ (20 ng/ml), CpG (1 nmol/ml), or PolyI:C (50 μg/ml).

2.4 | Cell sorting

For isolation of primary microglia for transcriptome analysis, cells were stained with CD11b-PE (AB_396680) and DAPI as live-dead dye and 1×10^4 to 2×10^4 cells sorted on a BD FACS Aria III (BD Biosciences) using a 100 μM nozzle and subsequently lyzed in 1 ml Qiazol (Qiagen).

2.5 | RNA preparation for sequencing

For RNA isolation, total RNA was extracted from primary microglia using a miRNeasy micro Kit (Qiagen) according to the manufacturers' recommendations. Total RNA was eluted in RNAse free water. The quantity and quality of the RNA was assessed by an RNA assay on a Tapestation 4200 system (Agilent).

2.6 | Library preparation for RNA sequencing

Samples with more than 100 ng total RNA were converted into NGS libraries using the TruSeq RNA Library Prep Kit v2 (Illumina) at 100 ng input according to manufacturer's recommendations. The size-distribution of the libraries was determined using the Agilent D1000 assay on a Tapestation 2200 system (Agilent). Libraries were quantified using a Qubit HS dsDNA assay. 75 bp single-end sequencing was performed on a HiSeq1500 system using Rapid v2 chemistry. Base calling from base call files and demultiplexing was performed with CASAVA v1.8 (Illumina).

Low input Samples were converted into libraries of double stranded cDNA molecules as a template for high throughput sequencing following the SMART-Seq2 protocol. Shortly, mRNA was primed for SMART reverse transcription from 5 ng of total RNA using poly-T oligos. cDNA was pre-amplified by SMART ISPCR. Fragmentation was performed using the Illumina Nextera XT kit, followed by PCR amplification and indexing. Size-selection and purification of library

fragments preferentially 300–400 bp in length was performed using SPRIBeads (Beckman-Coulter). The size-distribution of cDNA libraries was measured using the Agilent high sensitivity D5000 assay on a Tapestation 4200 system (Agilent). cDNA libraries were quantified using a Qubit high sensitivity dsDNA assay. 75 bp single-end sequencing was performed on a NextSeq500 system using High Output v2.5 chemistry. Base calling from base call files, alignment to the *Mus musculus* reference genome mm10 from UCSC and file conversion to fastq files were achieved by Illumina standard pipeline scripts (STAR version, bcl2fastq2 v.2.20).

2.7 | RNA sequencing analysis

Kallisto l (Bray, Pimentel, Melsted, & Pachter, 2016) was used to quantify abundances of transcripts from the bulk RNA-seq data. Raw kallisto files were imported using tximport (Soneson, Love, & Robinson, 2015) and DESeqDataSetFromTximport function from DESeq2 (v1.26.0) (Love, Huber, & Anders, 2014) and rlog transformed according to the DESeq2 pipeline. DESeq2 (based on a model using negative binomial distribution) was used for the calculation of normalized counts for each transcript using default parameters. All normalized transcripts with a maximum over all row mean lower than 10 were excluded resulting in 23,995 present transcripts. Differentially expressed genes were calculated for CpG_wt versus Unstim_wt, Poly_IC_wt versus Unstim_wt, LPS_IFNγ_wt versus Unstim_wt, CpG_CB2$^{-/-}$ versus Unstim_CB2$^{-/-}$, Poly_IC_CB2$^{-/-}$ versus Unstim_CB2$^{-/-}$, LPS_IFNγ_ CB2$^{-/-}$ versus Unstim_ CB2$^{-/-}$, Unstim_ CB2$^{-/-}$ versus Unstim_wt, CpG_ CB2$^{-/-}$ versus CpG_wt, Poly_IC_ CB2$^{-/-}$ versus Poly_IC_wt, LPS_IFNγ_ CB2$^{-/-}$ versus LPS_IFNγ_wt separately using a *p*-value cutoff of .05, an adjusted *p*-value (IHW) < .05 (independent hypothesis weighting), and an FC threshold of 1.5. All present transcripts were used as input for principal component analysis. The top 25% most variable transcripts within the dataset were selected and visualized in a heat map. Hierarchical clustering on the columns was performed using Euclidean distance and ward.D2 as agglomeration method.

Date of experiment was modeled as a known batch factor using the "Linear Models for Microarray and RNA-Seq Data" (Limma) package (Ritchie et al., 2015).

The top 15,000 variable genes were selected and used as an input for co-expression network analysis using CoCena2 (https://github.com/UlasThomas/CoCena2). Pearson correlation analysis was performed with correlational significance measure *p* < .05 and correlation coefficient cut-off of 0.888 and a R^2 of 0.832 leading to 4792 genes and 130,118 edges. Based on Louvain community detection algorithm 7 modules were identified based on the expression pattern in the dataset. Clustering was repeated 20 times.

Utilizing the R package clusterProfiler, CoCena2 automatically analyzes the gene modules with respect to different kinds of gene set enrichments: the genes within each module are compared against the database KEGG (Kanehisa, 2000), Hallmark (Liberzon et al., 2015), Gene Ontology (Blake et al., 2015), and Reactome (Fabregat et al., 2016). Using the R ChEA3 (Keenan et al., 2019), the genes were also analyzed

for the enrichment of transcription factor binding sides, and if the predicted transcription factors are present in the data. The top five predicted TFs and targets combination were visualized as circos plots. Original data are available with the GEO number GSE173337.

2.8 | Filtering for transcription factors, epigenome, surfaceome, and secretome

All differentially expressed genes were filtered for one of the three categories and then for each stimulation (unstimulated, LPS/IFN-γ, PolyI:C and CpG) the top five downregulated and top five upregulated genes between CB2$^{-/-}$ and WT microglia were displayed in a scaled heatmap. Transcription factor lists were extracted from Fulton et al. (Fulton et al., 2009), the epigenome gene list was literature-driven, and surface and secretome markers were extracted from the Human Protein Atlas (Uhlén et al., 2015).

2.9 | Immunohistochemistry

OHSC of 350 μm thickness were stained with primary anti-mouse antibodies diluted 1:1000 for 3 days at 4°C. Incubation with the secondary antibody (diluted 1:1000) was performed for 5 h at 4°C, followed by staining with 4′,6-diamidino-2-phenylindole DAPI. Antibodies used were Iba1 (AB_839504), CD68 (AB_322219), Goat-anti-rabbit AF488 (AB_143165) and Goat-anti-rat AF647 (AB_141778).

Images were taken with a confocal laser scanning microscope (63×) (Leica TCS SP8). For microglial analysis, z-stacks were taken with a step size of 1 μm.

2.10 | Microglial cell reconstruction and analysis of microglial morphology

Microglial morphology was quantified using a custom-written ImageJ toolbox designed to reconstruct and analyze microglial cells, similarly to previous studies from Plescher et al and Schmöle et al (Plescher et al., 2018; Schmöle et al., 2018). The toolbox consists of three ImageJ plugins for single-cell image generation, image segmentation and cell analysis. Per group in each genotype, at least 50 activated microglial cells (as identified as Iba1$^+$ CD68$^+$ [Yousef et al., 2019]) were selected in all z-slices of confocal z-stacks by an investigator that was blind to the experimental conditions using the single-cell selection plugin. The resulting single-cell images were segmented using the image segmentation plugin. An intensity threshold (algorithm: "Huang") was calculated in an 8-bit converted, 0.5-fold scaled and maximum-intensity projected copy of the original image. The threshold was applied to the unmodified original image. Segmented images were analyzed using the cell analysis plugin after applying a particle-filter > = 100 voxel. The microglial mean Iba1 intensity was determined as the mean intensity of all voxels in the original image that were positive in the particle-filtered, segmented image. The 3D

microglial ramification index was defined as: cell surface area/(4π × [(3·cell volume)/(4π)]$^{(2/3)}$), which describes the ratio of cell surface to cell volume and serves as a sensitive measure for cell shape complexity. To determine the "Branch number" and "Tree length", the segmented images, after particle filtering, were Gauss-filtered (Sigma XY = 1.0 and Sigma Z = 0.0), skeletonized using the Fiji plugin "Skeletonize3D" (Arganda-Carreras, Fernández-González, Muñoz-Barrutia, & Ortiz-De-Solorzano, 2010) and analyzed using the Fiji plugin "Analyze Skeleton" (Arganda-Carreras et al., 2010). The polarity index indicates how equally the process tree is distributed around the cell soma. It was defined as the length of the vector from the center of mass of the microglial cell to the center of the convex hull around the microglial cell, normalized to the size of the convex hull: polarity index = vector length/(2 × $\sqrt[3]{3 \cdot \text{spanned volume}/(4\pi)}$).

The size of the cell soma was determined in ImageJ as follows:

1. A maximum intensity projection was created for the z-stack containing the analyzed cell;
2. A trained user encircled the cell soma with the free-hand tool in ImageJ;
3. The area of the selection was calculated in ImageJ, which was used as a measure for the soma size.

Activated microglia were identified by Iba1- and CD68-immunoreactivity.

2.11 | Flow cytometry

Stimulated BM-derived macrophages were harvested and blocked with CD16/32 antibodies as Fc-receptor blocker. Subsequently, cells were stained with CD11b-e450 (AB_1582236), CD40-APC (AB_469386), ICAM1-FITC (AB_465095), CD45-Bio (AB_312969), and MHC II-PE (AB_313322). Bio-tagged antibody markers with Streptavidin PerCP-Cy5.5 (AB_2868934) were used as secondary antibodies.

Acquisition and analysis were performed on a FACSCanto (BD Biosciences) and FlowJoTM software (Tree Star, Ashland, OR).

2.12 | ELISA

The murine IL-6, tumor necrosis factor α (TNFα) and CC-chemokine ligand (CCL) 2 Ready-SET-Go! ELISA kits (eBioscience) were used to quantify the levels of these cytokines in BM-derived macrophage cell culture supernatants. Quantitative determination was carried out according to manufacturer's protocol.

2.13 | Protein isolation

Microglia cells harvested after the stimulation periods were lysed in RIPA buffer (10 mM Tris pH 8.0, 150 mM NaCl, 1% deoxycholate, 1% NP-40, 0.1% SDS, 5 mM EDTA pH 8.0) containing protease inhibitors and phosphatase inhibitors (Thermo). The protein content of the lysate was concentrated using Amicon centrifugal filters with a 100 kDa cutoff. Total protein concentration of the retentate lysates were then determined using BCA kit (Thermo).

2.14 | Western blotting

Western blotting analysis was performed on a Wes system (ProteinSimple, San Jose) according to the manufacturer's instructions using a 12–230 kDa Wes/Jess Separation Module and the Anti-Rabbit Detection Module. Antibodies against p38 MAPK (AB_3303713) (1:500 dilution), phospho-p38 MAPK (T180/Y182) (AB_2139682) (1:3 dilution) and β-actin (AB_10001612) (1:5000 dilution) (rabbit, Novus Biologicals) were used. Secondary antibody was HRP-conjugated anti-rabbit (AB_2860577) (Protein Simple).

2.15 | Statistical analysis

Data are expressed as mean ± SEM. Statistical analysis was performed used was Graph Pad Prism Software Version 7.0. Two way analysis of variance (ANOVA) followed by Bonferroni's post hoc test was used to analyze the genotype and treatment statistical comparison between groups.

3 | RESULTS

3.1 | CB2$^{-/-}$ microglia show reduced TLR signaling

To better understand the contribution of CB2 signaling to microglia activation we employed an in vitro experimental system. Therefore, primary neonatal microglia derived from WT and CB2$^{-/-}$ mice were stimulated for 16 h in vitro with LPS/IFN-γ, PolyI:C or CpG to activate TLR4, TLR3, and TLR9, respectively (Figure 1(a)). We chose three different TLRs as they represent both membrane (TLR4) and lysosomal TLRs (TLR3, 9) and act via MyD88 and/or TRIF/TRAM signaling. By this we aimed to identify pathway-specific or conserved alterations influenced by CB2 during microglial activation.

Subsequent bulk RNA-seq analysis revealed significant differences in gene expression between the two genotypes in steady state and especially upon activation. A principal component analysis showed that the first principal component separates the samples based on the different stimuli whereas the second component clearly splits the samples by genotype (Figure 1(b,c)). The same clear pattern of separation can be appreciated upon hierarchical clustering based on the top 25% variable genes (Figure S1a), suggesting an important role for CB2 signaling during TLR ligand induced microglial activation.

This also became evident, when assessing differentially expressed genes (DEG) between unstimulated and stimulated WT microglia, as a strong response was observed when WT microglia were stimulated
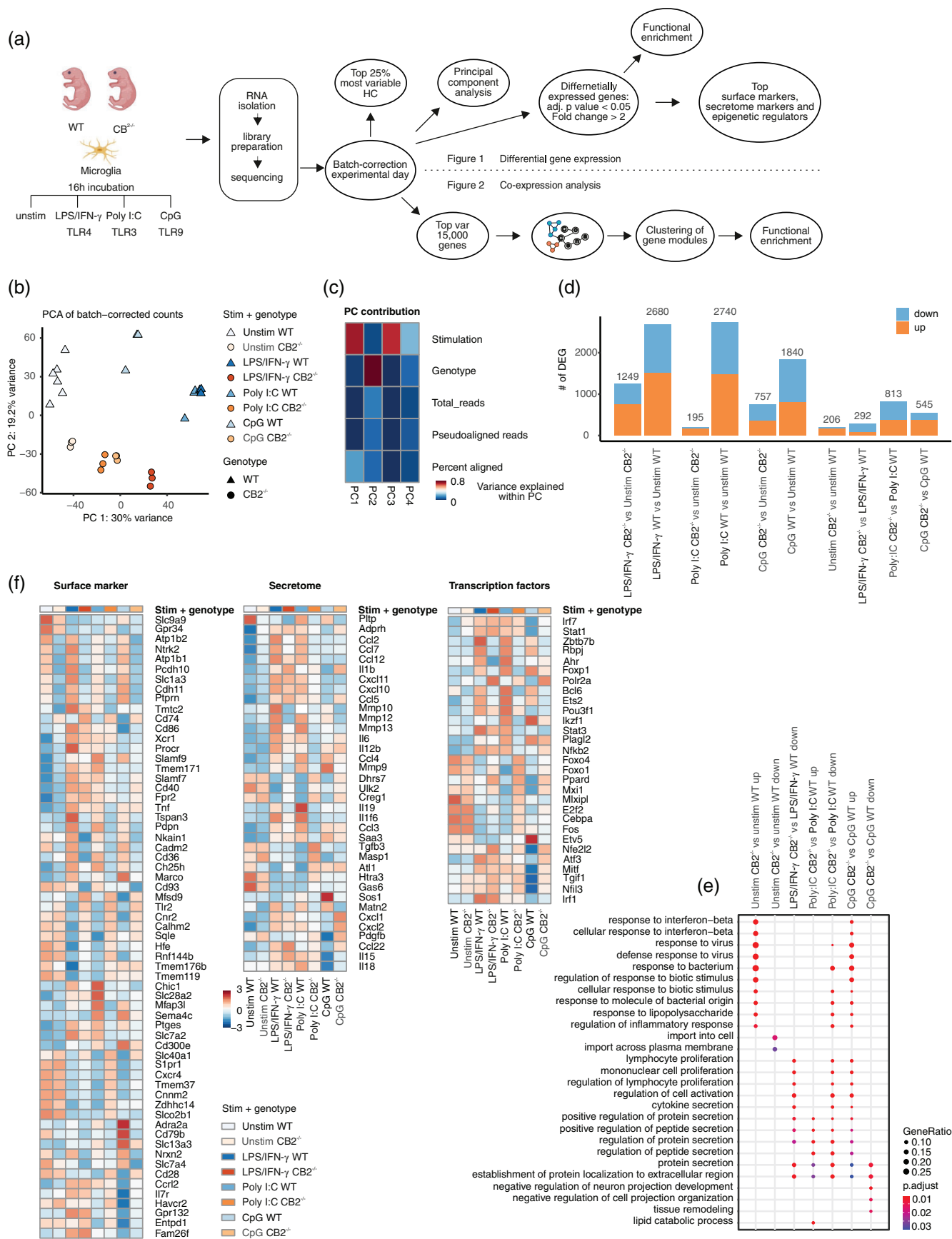
FIGURE 1 Legend on next page.

with the different TLR stimuli. However, this response was reduced by half in LPS/IFN-γ and CpG stimulated microglia (2680 VS 1249 DEG in LPS/IFN-γ and 1840 VS 757 DEG in CpG). The response of CB2$^{-/-}$ microglia to PolyI:C was almost completely lost with only 195 genes from 2740 genes in WT microglia still differentially expressed after loss of CB2 (Figure 1(d)). Next, we compared changes between CB2$^{-/-}$ and WT microglia for each stimulatory condition. As expected from the comparison of the stimulation-dependent DEG, we identified a small but significant number of DEG for each stimulation condition (206 in unstimulated, 292 in LPS/IFN-γ, 813 in PolyI:C and 545 DEG in CpG stimulated microglia; Figure 1(d)). In unstimulated and CpG stimulated microglia most of these DEG were upregulated, whereas, in line with the aforementioned results, in LPS/IFN-γ and PolyI:C stimulated microglia most DEG were downregulated. To better understand which biological processes were impacted by the loss of CB2, we performed a gene ontology (GO) analysis. This revealed an upregulation of the GO term "response to interferon-beta" in the unstimulated microglia when comparing CB2$^{-/-}$ versus WT microglia which persisted in the comparison across the CpG stimulated microglia (Figure 1(e)). In CpG stimulated microglia, deletion of CB2 additionally leads to a cell activation signature together with upregulation of the GO terms "cytokine secretion" and "protein secretion". The term "negative regulation of cell projection organization" on the other hand was downregulated in the CB2$^{-/-}$ microglia, altogether supporting a pre-activated or primed microglial state poised for a direct response in CB2-deficient microglia. For the other two TLR stimuli the GO terms are rather associated with a downregulation of immune activation in CB2$^{-/-}$ microglia. The term "protein secretion" is enriched in PolyI:C stimulated microglia of CB2$^{-/-}$ mice together with "lipid catabolic processes", but the terms for" regulation of cell activation", "cytokine secretion" and multiple terms concerning anti-viral and anti-bacterial response are all downregulated in CB2$^{-/-}$ microglia as compared to WT microglia. For the LPS/IFN-γ stimulation no GO terms were associated with the upregulated genes, but in line with the observations for PolyI:C stimulated microglia, GO terms for "regulation of cell activation", "cytokine secretion" and "protein secretion" are downregulated. These results support that CB2 is required for the full activation spectrum downstream of TLR3 and TLR4 activation in microglia. Next, we were interested in functional aspects and upstream regulators altered by the loss of CB2. Therefore, we assessed genes implicated in the surfaceome and secretome or described as transcription factors (TF). DEG in these categories included interesting genes such as *Cd36*, *Marco*, *Cd79b* for the surfaceome, *Mmp10/12/13*, *Il6*, *Ccl3* and *Sos1* for the secretome and

finally TF like *Ahr*, *Foxp1* and *Stat3* that are differentially regulated upon stimulation between CB2$^{-/-}$ and WT microglia (Figure 1(f)). Interestingly, *Irf7* and *Stat1* are upregulated in steady state and after CpG stimulation upon loss of CB2, supporting a distinct program mediated by CB2 in unstimulated and TLR9 activated microglia leading to a pre-priming of microglia in contrast to the loss of the full activation spectrum downstream of TLR3/4 signaling.

Taken together, CB2 deficiency leads to an upregulation of interferon response genes and cell activation gene signatures in steady-state and CpG-stimulated microglia, whereas the activation of an antimicrobial response signature and cytokine secretion is lost in the absence of CB2 upon LPS/IFN-γ and PolyI:C stimulation supporting a dampening of transcriptional activity mediated by CB2.

3.2 | Co-expression analysis reveals disruption of MAPK signaling in CB2$^{-/-}$ microglia

To find common pathways influenced by CB2 across the different TLR stimuli, we conducted a co-expression analysis (Figure 2(a)). We were able to identify seven significantly co-expressed modules of genes that differed between the different experimental conditions. The group-fold change (GFC) of each module for each condition shows distinct patterns (Figure 2(b)). The module dark green is specific for unstimulated microglia from both WT and CB2$^{-/-}$ and the PolyI:C stimulated CB2$^{-/-}$ microglia. Comparing the enrichment of this module between unstimulated CB2$^{-/-}$ and WT microglia supports a slight downregulation in CB2-deficient microglia. Cluster steel blue is shared between unstimulated and CpG-stimulated WT microglia. All three TLR stimuli show a specific enrichment for clusters dark orange and orchid that are dramatically reduced upon loss of CB2 and are potentially responsible for the reduced activation downstream of TLR3/4 observed in CB2-deficient microglia. Cluster dark gray is upregulated upon LPS/IFN-γ and PolyI:C stimulation in WT microglia and in LPS/IFN-γ stimulation of CB2$^{-/-}$ microglia, but downregulated upon loss of CB2 in PolyI:C stimulated microglia, supporting a major influence of this cluster on the observed changes induced by loss of CB2 on transcriptomic level between LPS/IFN-γ and PolyI:C stimulation (Figure 1(d)). The gold and maroon clusters are exclusively upregulated in all CB2$^{-/-}$ microglia supporting that CB2-dependent genes are enriched in these modules.

To further support this hypothesis, we asked whether the DEG from the comparisons of CB2$^{-/-}$ versus WT microglia across all TLR stimuli are represented in the co-expression modules. In total,

FIGURE 1   Microglia transcriptional response to TLR4/3/9 stimulation is dampened in CB2$^{-/-}$ mice. Primary neonatal microglia from WT and CB2$^{-/-}$ mice were stimulated for 16 h with control medium (WT: N = 6; CB2$^{-/-}$: N = 3), LPS/IFN-γ (WT: N = 3; CB2$^{-/-}$: N = 3), PolyI:C (WT: N = 3; CB2$^{-/-}$: N = 3) or CpG (WT: N = 3; CB2$^{-/-}$: N = 3) to stimulate TLR-4, 3, or 9, respectively and underwent subsequent bulk RNA-seq and bioinformatic analysis (a). Principal component analysis of all samples reveals a separation by stimulation in the first dimension and a separation of the samples by genotype in the second dimension (b) Variability of principal components explained by metadata of the samples (c). Differential genes (DEG) were defined by a fold-change of 1.5 and an adjusted *p*-value <.05 showing clear differences between WT and CB2$^{-/-}$ (d). Most significant GO terms based on DEG between WT and CB2$^{-/-}$ for each stimulation (e). Heatmaps of specific functional groups of genes displaying the Top10 DEG for each condition (f). Parts of this figure were created with Biorender

FIGURE 2   Legend on next page.

70 genes (40 down- and 30 upregulated; Figure S2a) are shared across all three comparisons. Of these 70 genes, 65 are represented in the co-expression analysis, with upregulated genes mainly represented in the dark green, maroon and gold clusters and the downregulated genes in the dark orange and orchid clusters (Figure 2(c)). As the dark gray and steel blue clusters only contain 2 and 3 of these core genes, respectively it is highly conceivable that this is not representative. A heatmap of the union of all DEG identified for the three TLR stimuli revealed that most of the upregulated genes belong to the dark green and maroon clusters, whereas the genes downregulated in CB2$^{-/-}$ microglia belong to the orchid and dark orange clusters (Figure S2b). Interestingly, the dark green cluster is highly enriched for genes that are upregulated in PolyI:C-stimulated CB2$^{-/-}$ microglia (Figure 2(d)). Cluster maroon consists of genes from both PolyI:C and CpG-stimulated CB2$^{-/-}$ microglia. Many genes from the steel blue cluster are downregulated in unstimulated or LPS/IFN-γ or CpG stimulated CB2$^{-/-}$ microglia. Clusters dark orange and orchid are dominated by genes that are downregulated in CB2-deficient microglia upon PolyI:C treatment. Cluster dark gray is highly enriched for genes upregulated in unstimulated or CpG-stimulated CB2$^{-/-}$ microglia. Cluster gold is dominated by genes upregulated in CpG, but downregulated in LPS/IFN-γ and PolyI:C stimulated CB2$^{-/-}$ microglia. To link the co-regulated modules with biological functions, we performed GO and KEGG enrichment analysis and observed clearly enriched functions for each cluster (Figures 2(e,f) and S3). The dark green module is associated with the KEGG terms "PI3K-Akt signaling pathway" and "MAPK signaling pathway". The maroon module (specific for CB2$^{-/-}$ microglia) is enriched for the KEGG term "lysosome" and the GO term "response to oxidative stress" (Figure 2(e,f)). Interestingly, the maroon cluster contains *Cnr2*, the gene encoding CB2, among the co-expressed genes, further highlighting the correlation of CB2 expression with these terms (Figure S3). Cluster steel blue is associated with the GO term "generation of precursor metabolites and energy" (Figure 2(e)) and the KEGG term" Pathways of neurodegeneration - multiple diseases" (Figure 2(f)). Cluster dark orange is highly specific for TLR-dependent stimulation of WT microglia and is associated with the GO term" positive regulation of cell adhesion", but also "positive regulation of cell activation". Cluster orchid is of high interest as it is not only enriched specifically in the WT microglia after TLR stimulation, but also encompasses the GO terms "positive regulation of cytokine production", "positive regulation of cell adhesion" and most interestingly KEGG terms around neurodegenerative diseases like "Parkinson's disease", "Amyotrophic lateral sclerosis" or "Alzheimer disease" supporting that this cluster contains crucial genes associated

with TLR3/4 mediated activation of microglia which are influenced by CB2 signaling and could be most relevant for the observed impact of loss of CB2 on AD pathology as reported before (Schmöle et al., 2018; Schmöle, Lundt, Ternes, et al., 2015). This cluster also contains TF associated with TLR signaling like *Nfkb1* and *Nfkb2*, but also *Cd274* and *Tnf* as surface markers (Figure S3) and includes most of the conserved genes downregulated upon CB2 depletion (Figure S2b). The dark gray cluster is enriched for the GO term "defense response to virus" with additional terms associated with this cluster like "positive regulation of cytokine production" and is mostly conserved in the LPS-stimulated cells, but completely lost in the PolyI:C stimulated CB2$^{-/-}$ microglia. This cluster contains TF specific for an anti-viral immune response like *Irf1*, *Stat1* and *Irf7* which not only are enriched in unstimulated and CpG-activated CB2$^{-/-}$ microglia, but whose activation is prevented by loss of CB2 upon PolyI:C stimulation (Figure 1(f)). Finally, cluster gold is specific for all CB2$^{-/-}$ microglia and is connected to GO terms like "negative regulation of immune system process", but also the KEGG terms" HIF-1 signaling pathway" and "cellular senescence" and contains genes which are influenced in general by the loss of CB2 and are shared among CB2-deficient microglia (Figures 2(c,d) and S2b). Next, we were interested to better understand how loss of CB2 would influence the activity of all three distinct TLR ligands. Therefore, we focused on the clusters dark orange and orchid displaying the strongest difference between activated CB2 deficient and WT microglia. When displaying the genes of the shared GO term "positive regulation of cell adhesion" as a heatmap (Figure 2(g)) we observed a distinct transcriptional regulation upon TLR3 and TLR4 stimulation in WT which is missing in CB2$^{-/-}$ microglia. This suggests that loss of CB2 prevents morphological adjustments upon TLR stimulation.

3.3 | CB2$^{-/-}$ microglia show altered morphology after TLR-activation

We next used organotypic hippocampal slice cultures (OHSC) as a model of microglial activation in an in vivo-related situation to further address the role of CB2 signaling for the modulation of TLR responses (Figure 3(a)).

The genes of the GO term "positive regulation of cell adhesions" were induced after TLR-stimulation in WT but not in CB2$^{-/-}$ microglia. Early studies have shown that the increase in adhesion molecules such as integrins has been associated with transition into ameboid microglia upon activation (Kim et al., 2014; Milner &

FIGURE 2 Co-expression network analysis of transcriptional response to TLR-4/3/9 stimulation. Co-expression analysis based on the most variable genes revealed 7 major modules that can be associated with specific biological functions (a). Heatmap of group fold-changes (GFC) reveals differential expression across the different experimental conditions for each module (b). Below the core signature genes (c) from (S2a) as well as the DEG for each comparison of CB2$^{-/-}$ versus WT microglia within a stimulation (d) are enriched for each cluster. The number indicates how many genes from the respective module are found in the conserved genes or DEG. The stacked bars indicate the frequency of genes derived from each signature. The Top5 GO (e) and KEGG terms (f) for each module reveal specific biological functions for each module. Heatmap of the genes from the GO term "positive regulation of cell adhesion" with the mean expression for each condition scaled by rows (g)
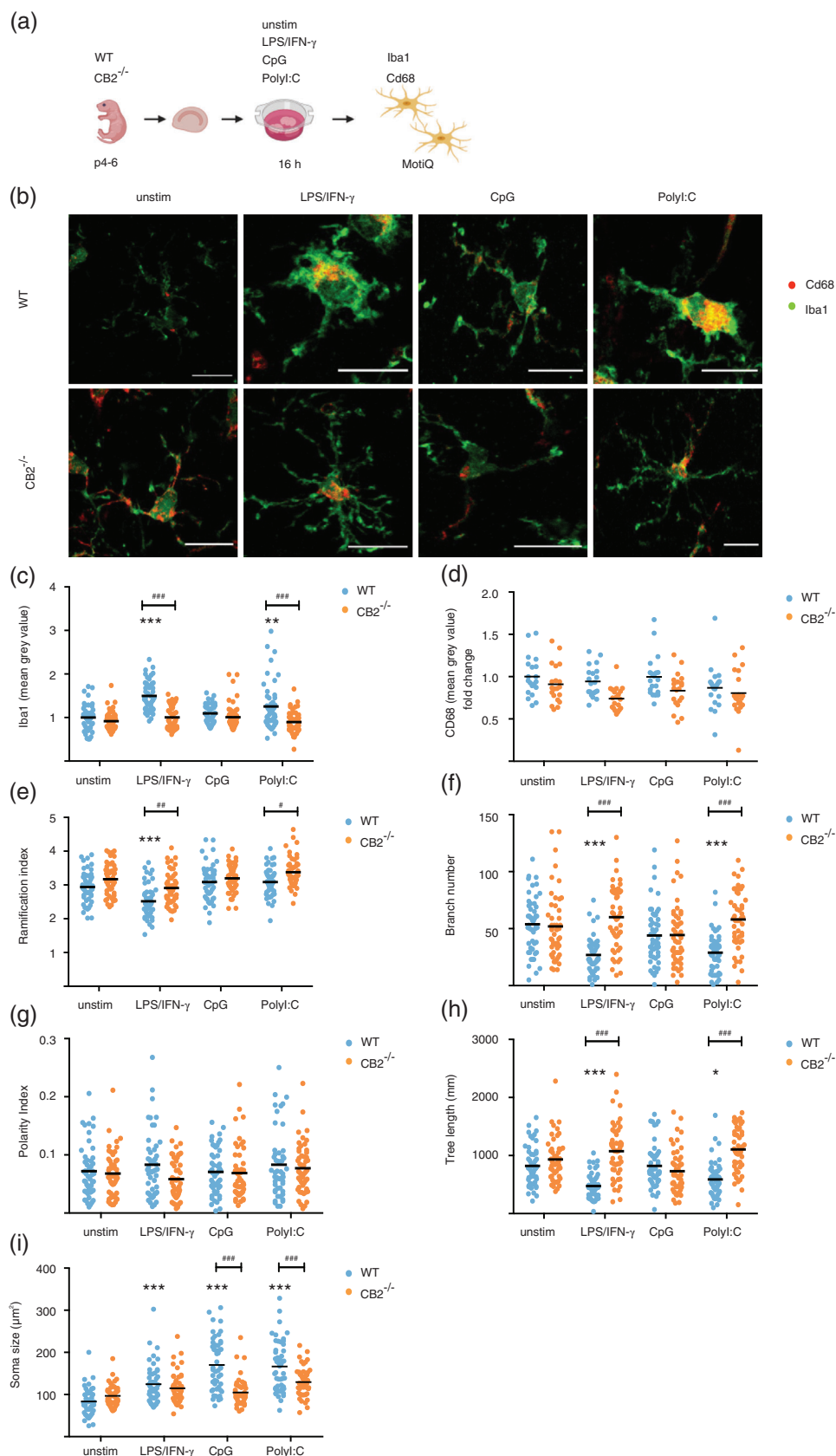
FIGURE 3 Microglia morphology analysis in OHSC from WT and CB2$^{-/-}$ mice after TLR stimulation. Experimental setup (a) and representative microscopy images with a scale bar of 20 μm (b). Iba1 intensity was higher in WT microglia when compared to CB2$^{-/-}$ microglia (genotype effect: Iba1 F$_{1,392}$ = 68.05, *p* < .001; CD68 F$_{1,389}$ = 38.69, *p* < .001) (c) whereas CD68 intensity was not changed (d). Microglia morphology was analyzed by measuring the ramification index (e), branch numbers (f), polarity index (g), tree length (h) and soma size (g). All analyzed parameters showed a significant genotype effect (ramification index F$_{1,390}$ = 30.78, *p* < .001; polarity index F$_{1,392}$ = 4.001, *p* < .05; branch numbers F$_{1,389}$ = 38.69, *p* < .001; junction numbers F$_{1,389}$ = 37.95, *p* < .001; tree length F$_{1,387}$ = 61.18, *p* < .001, soma size F$_{1,392}$ = 33.68, *p* < .001). Data are displayed as mean. Two-way ANOVA followed by Bonferroni's multiple comparisons with #*p* < .05, ##*p* < .01, ###*p* < .001, *significance to corresponding genotype control. Parts of this figure were created with Biorender

Campbell, 2003). We thus analyzed microglial morphology as defined by ramification, branch numbers, polarity index, tree length and soma size in OHSC from WT and CB2$^{-/-}$ mice stimulated with LPS/IFN-γ, CpG and PolyI:C. We stained for the microglial marker, Iba1 and the phagocytic marker, CD68 (Figure 3(b)) to identify activated microglia. Subsequently, we measured Iba1 and CD68 intensity to assess

microglia activation. Statistical analysis revealed that Iba1 (Figure 3(b, c)) and CD68 intensity (Figure 3(b,d)) were greater in WT microglia when compared to CB2$^{-/-}$ microglia.

Using the ImageJ plugin MotiQ to determine microglia morphology in OHSC from WT mice, we observed that WT microglia were less ramified, had fewer branches, shorter trees and larger somas after stimulation with LPS/IFN-γ than unstimulated control cells (Figure 3 (e,f,h,i)), whereas cellular polarity was unaffected. Similar effects were observed after stimulation with PolyI:C, whereas stimulation with CpG only increased soma size (Figure 3(c–i)). In contrast, microglia from CB2$^{-/-}$ mice showed no change in morphology as a consequence of TLR stimulation as well as no Iba-1 or CD68 increase suggesting that the microglia are less activated (Figure 3(c–i)). These data support the hypothesis from the gene expression that the loss of CB2 affects microglia morphological changes induced by TLR-dependent activation.

3.4 | BM-macrophages from CB2$^{-/-}$ mice are less responsive to TLR-stimulation

To investigate if the CB2-mediated dampening of the inflammatory response to TLR stimulation is specific for microglia, or also occurs in other myeloid cells, we analyzed how CB2-deficient bone marrow derived macrophages (BMDM) react to TLR-stimulation (Figure 4(a)).

Therefore, BMDM from WT and CB2$^{-/-}$ mice were stimulated with LPS/IFN-γ, CpG and PolyI:C and subsequently inflammatory markers including cell surface markers like CD40, ICAM and MHCII (Figure 4(b–d)) and cytokines like TNFα, CCL2 and IL6 (Figure 4(e–g)) were analyzed.

In line with the observations on transcriptome level for microglia, stimulation of WT BMDM with LPS/IFN-γ or PolyI:C resulted in increased expression of inflammatory cell surface markers CD40 and ICAM, whereas stimulation with CpG had no effect (Figure 4(b,c)). In contrast, expression of both CD40 and ICAM was significantly reduced on CB2$^{-/-}$ BMDM (Figure 4(b,c)) while expression of MHCII was only slightly downregulated after TLR-stimulation on CB2$^{-/-}$ BMDM (Figure 4(d)).

Next, we determined the release of TNFα, CCL2, and IL6 by WT BMDM and could observe a significant enhancement after stimulation with LPS/IFN-γ and PolyI:C. In line with our findings for cell-surface activation markers, the release of TNFα, CCL2, and IL6 by WT BMDM was not enhanced after stimulation with CpG. The deletion of CB2 caused a significant reduction of LPS/IFN-γ - induced release of TNFα compared to WT BMDM (Figure 4(e)). In contrast, no difference in the LPS/IFN-γ - induced release of CCL2 or IL6 could be observed between WT and CB2$^{-/-}$ BMDM. In line with this, CB2 deletion did not affect the PolyI:C-induced secretion of TNFα, IL6 and CCL2 (Figure 4(e–g)). Taken together, BMDM from CB2$^{-/-}$ mice also show a dampened inflammatory response to TLR-stimulation which is not as pronounced as in CB2$^{-/-}$ microglia and support a model, where only very specific aspects of microglia and myeloid cell activation are impacted by the loss of CB2.

3.5 | CB2-dependent changes in TLR-induced microglial activation are mediated by p38

Next, we wanted to elucidate the molecular mechanism that prevents TLR-mediated microglia activation in the absence of CB2 (Figure 5(a)). Previous studies demonstrated that CB2 receptor activity influences MAPK kinase activity, but also interferes with the Janus kinase (JAK)/ signal transducers and activators (STAT1) pathway (Bouaboula et al., 1996; Ehrhart et al., 2005; Montecucco & Burger, 2008). This is supported by the co-expression analysis of the gene expression data which revealed strong differences between WT and CB2$^{-/-}$ microglial gene expression in the KEGG terms "PI3K-Akt signaling pathway" and "MAPK signaling pathway" (Figure 2(b,e–f)).

To investigate a possible involvement of MAPK signaling we visualized the expression of the KEGG pathway "MAPK signaling" as a heatmap over all conditions after 16 h of TLR stimulation to show that steady-state activity of the pathway is diminished upon CB2 deletion in unstimulated microglia (Figure 5(b)). Additionally, MAPK signaling is upregulated in LPS/IFN-γ and Poly I:C stimulation in WT, but not CB2$^{-/-}$ microglia. To support this hypothesis, we analyzed the gene expression of the p38 encoding genes *mapk11-14* as well as the phosphorylation of p38 MAPK in neonatal microglia from WT and CB2$^{-/-}$ mice (Figure 5(a)).

While expression of *mapk12* and *mapk13* was below the detection levels (data not shown), expression of *mapk11* is enhanced after 16 h of stimulation with LPS/IFN-γ, CpG and PolyI:C (Figure 5(c)) in WT microglia. In contrast, this effect was not observed in microglia from CB2$^{-/-}$ mice. Next, we analyzed expression of *mapk14* as a potential regulator of the CB2 mediated dampening of TLR signaling. *Mapk14* was significantly reduced in WT microglia after stimulation with LPS/IFN-γ and CpG and to a slightly lower extent in PolyI:C treated WT microglia (Figure 5(d)). While CB2$^{-/-}$ microglia showed statistically significant downregulation of *mapk14* expression after TLR-stimulation, a trend towards lower expression was observed for all TLR ligands suggesting that CB2 could also be involved in the regulation of *mapk14* gene expression and could impact a fine-tuned response towards TLR-dependent regulation of its expression.

To determine changes also on protein levels, we subsequently measured phosphorylation of p38 after 30 min (Figure 5(f)) and after 16 h of TLR stimulation (Figure 5(e,g)) as changes in phosphorylation can both be very rapid events, but also sustained over prolonged periods of time. Stimulation with LPS/IFN-γ resulted in an enhanced p38 phosphorylation in WT microglia 30 min after stimulation. Similar results were also observed after stimulation with CpG and PolyI:C. Stimulation of CB2$^{-/-}$ microglia with different TLR agonists lead to similar trends, however, phosphorylation of p38 was in general much lower, and e.g. decreased by 70% in LPS/IFN-γ and by almost 90% in PolyI:C stimulated CB2$^{-/-}$ microglia compared to WT microglia, supporting a decreased activity of the MAPK pathway in CB2-deficient microglia. After 16 h, p38 phosphorylation levels were still significantly augmented in WT microglia after stimulation with LPS/IFN-γ and PolyI:C, but not after treatment with CpG (Figure 5(g)). The reduced reactivity upon TLR stimulation was still detectable in
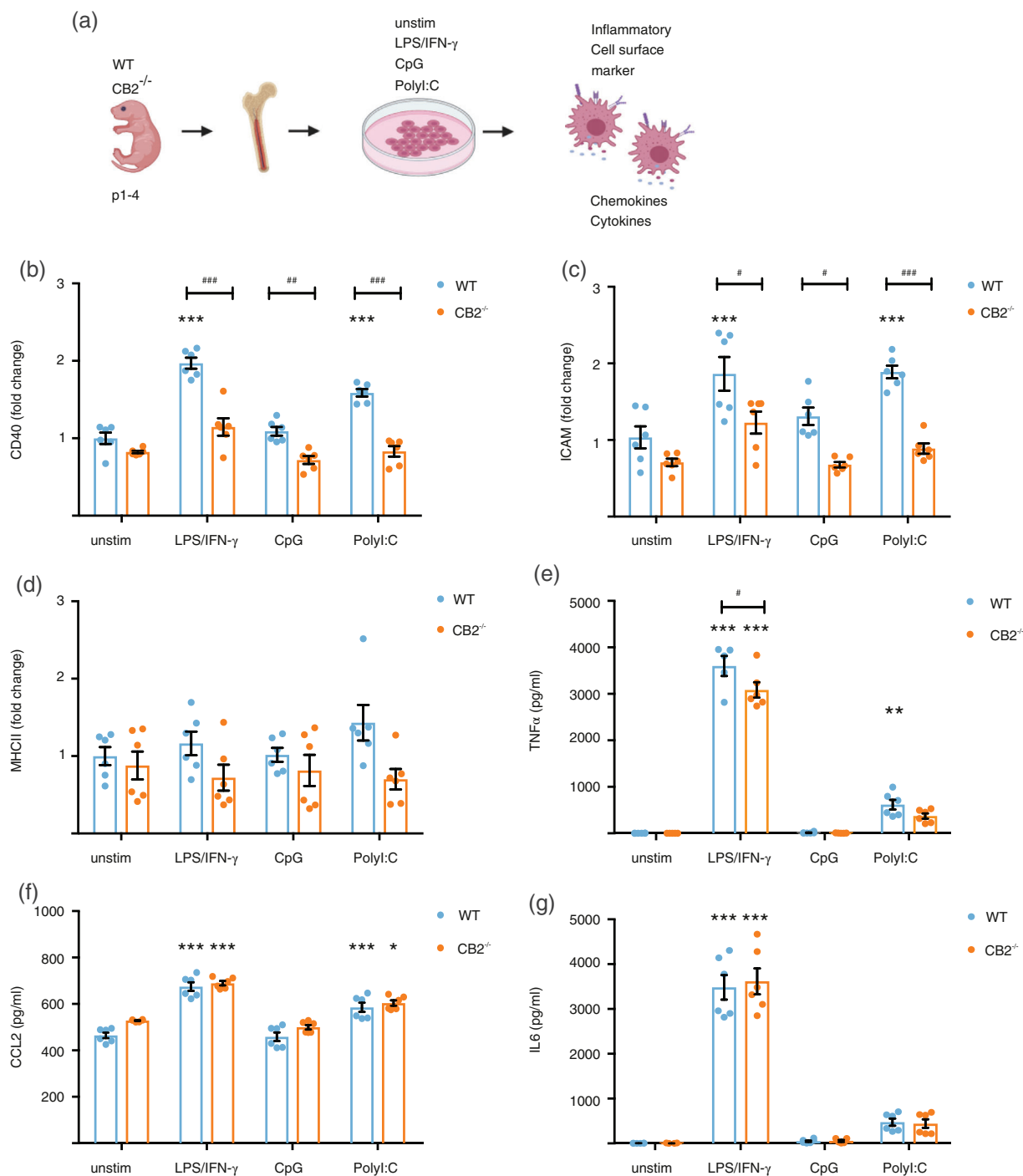
FIGURE 4 Inflammatory profile of BM-macrophages from WT and CB2$^{-/-}$ mice after stimulation with TLR ligands. Experimental setup (a). Expression of cell surface markers CD40 (b), ICAM (c) and MHCII (d), All analyzed surface markers showed a significant genotype effect (CD40 $F_{1,40}$ = 125.7, p < .001; ICAM $F_{1,390}$ = 57.09, p < .001; MHCII $F_{1,40}$ = 10.34, p < .01). Release of cytokines TNFα (e), CCL2 (f), IL6 (g) was enhanced after TLR stimulation (treatment effect, TNFα $F_{3,37}$ = 482.6, p < .001; CCL2 $F_{3,40}$ = 90.90, p < .001; IL6 $F_{3,37}$ = 235.4, p < .001). N = 3 independent experiments/genotype. Data displayed as mean ± SEM. Two-way ANOVA followed by Bonferroni's multiple comparisons with #p < .05, ##p < .01, ###p < .001, *significance to corresponding genotype control. Parts of this figure were created with Biorender

CB2$^{-/-}$ microglia as p38 phosphorylation levels were still significantly lower in CB2$^{-/-}$ microglia (decreased by 85% in LPS/IFN-γ stimulated CB2$^{-/-}$ microglia and by 80% in PolyI:C stimulated CB2$^{-/-}$ microglia) after 16 h, supporting that CB2 is required for the TLR3/4-mediated activation of microglia via MAPK signaling.

In summary, our data revealed that microglia lacking the CB2 receptor show a distinct gene expression profile after TLR-stimulation in line with a dampened microglial activation pattern. This was further supported by altered microglial morphology in CB2$^{-/-}$ OHSC. Similarly, also other myeloid cells, i.d. BMDM from CB2$^{-/-}$ mice, show a
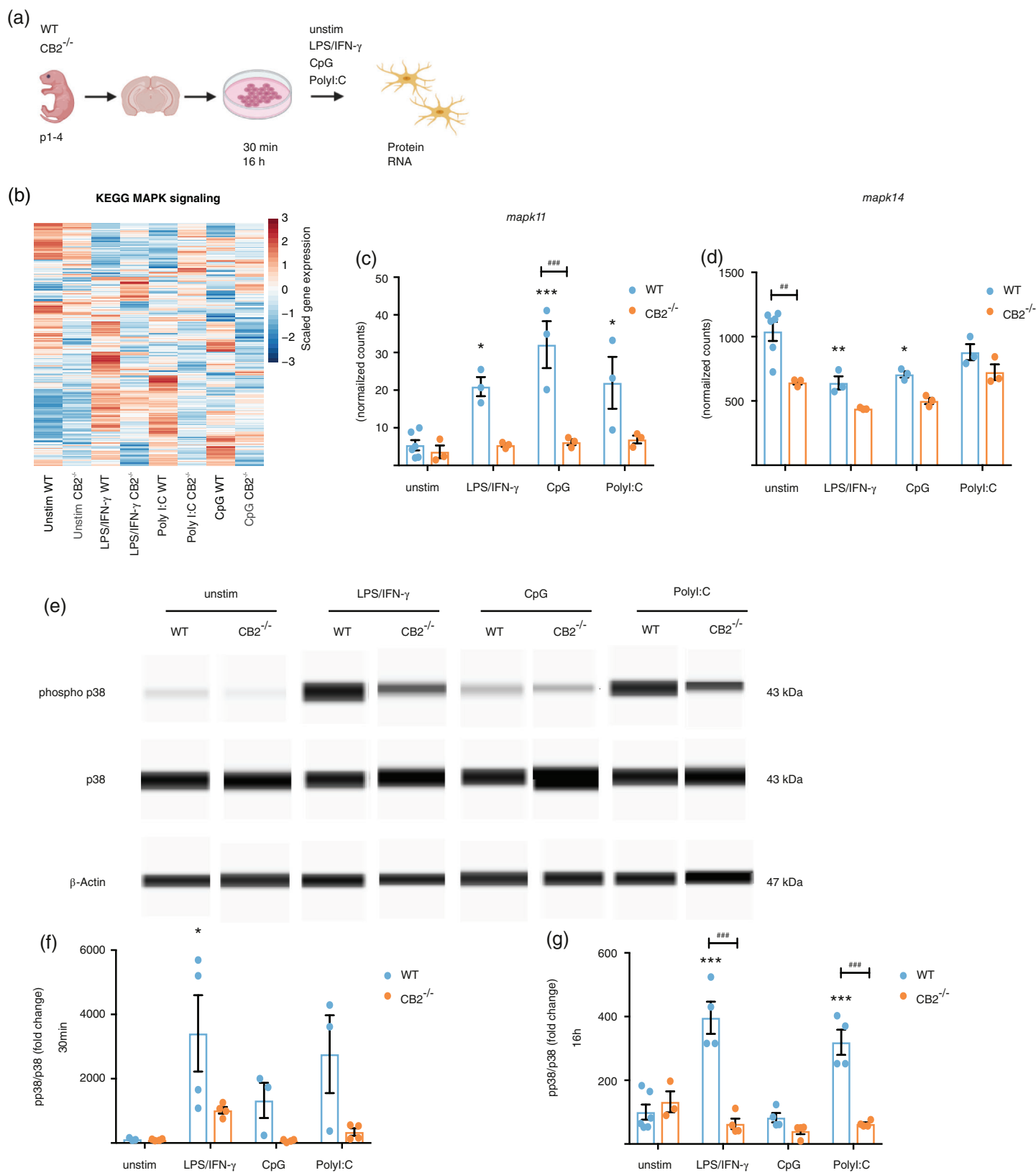
FIGURE 5 Legend on next page.

diminished response to TLR-stimulation, although less pronounced as in CB2$^{-/-}$ microglia. Mechanistically, we could demonstrate that phosphorylation of p38 MAPK was significantly reduced in CB2$^{-/-}$

microglia, suggesting that the expression of the CB2 receptor is necessary to allow for TLR-mediated p38 MAPK signaling promoting microglial activation.

4 | DISCUSSION

Here we provide new understandings of the control of TLR-mediated microglial action via the CB2 receptor. We demonstrate that microglia from CB2$^{-/-}$ mice are less responsive to TLR4 (LPS/IFN-γ) and TLR3 (PolyI:C) stimulation. The number of DEG induced by LPS/IFN-γ or PolyI:C was reduced by 50% or 90%, respectively, in microglia obtained from CB2$^{-/-}$ mice. Furthermore, we confirmed that CB2 deletion reduces TLR-induced microglial activation by morphological analysis of CB2-deficient microglia in OHSC. Finally, we identified p38 MAPK as a potential mediator that connects CB2 signaling to TLR-dependent microglial activation.

Using different types of TLR-stimuli, we delineated that CB2 deletion results in overall reduction in TLR-mediated microglial activation while the magnitude of the effect differs especially between TLR3/4 stimulation and TLR9 stimulation. At the same time, some aspects like alterations in microglial morphology were specific to TLR3/4 stimulation.

Stimulation of WT microglia with either LPS/IFN-γ (TLR4) or PolyI:C (TLR3) resulted in a pro-inflammatory gene expression profile including anti-viral response and cytokine production. In CB2$^{-/-}$ microglia these responses were drastically reduced, and the expression pattern was more similar to unstimulated microglia, especially in PolyI:C stimulated cells. On the contrary, TLR9 stimulation via CpG did not lead to a complete loss of pro-inflammatory signaling, but instead the cytokine secretion and anti-viral response was even slightly increased in the CB2$^{-/-}$ microglia, though in general the comparison between CpG and unstimulated microglia still led to less DEGs. Interestingly, the lack of CB2 in unstimulated primary microglia cultures led to a general upregulation of inflammatory gene signatures. The difference observed between the TLR stimuli guided us to the further analysis of the different signaling pathways. TLR3 and 4 share the TRIF/IRF3-dependent signaling pathway, whereas TLR9 transduces intracellular signaling via MyD88 and IRF7 (Fiebich et al., 2018). Therefore, it is possible that CB2 signaling interferes with TRIF or IRF3. Moreover, IRF7 is upregulated in CB2$^{-/-}$ microglia (Figure 1(e)). Our findings further support the proposed interaction of the endocannabinoid system with TRIF/IRF3 that was described in human macrophages (Downer et al., 2011). This study conclusively showed that CB1 and CB1/2 agonists modulated MyD88-independent signaling via TLR3 and TLR4 in human macrophages and inhibited IRF3 activation (Downer et al., 2011). Thus, our study provides further

evidence that not only CB1 on macrophages, but also microglial CB2 might be involved in TRIF/IRF3 interactions. However, as all the used CB1/2 agonists had a higher affinity to CB1, it cannot be excluded that the observed effects were influenced by CB1 signaling. Future studies should investigate the specific effect of the CB2 receptor on IRF3 since this is not conclusively shown so far.

It is widely accepted that changes in microglial morphology are tightly connected to their function and activation status. Activation of microglia results in increased Iba1 intensity accompanied by decreased cell ramification, less branch numbers and shorter trees. This is in line with previous studies where TLR-induced microglial morphological changes in OHSCs have been demonstrated already (Shaftel et al., 2007; Yousif et al., 2018). Correspondingly, we show that WT microglia in OHSC were less ramified, had less branches, shorter trees and larger somas after TLR3 and TLR4 stimulation. Together with the increased Iba1 intensity these data suggest that WT microglia get activated after TLR3 and TLR4 stimulation. In contrast, CB2$^{-/-}$ microglia showed no changes in morphology or Iba1 intensity after TLR stimulation. This indicates that CB2$^{-/-}$ microglia are less responsive to TLR stimulation and do not show an activated phenotype. Moreover, CB2$^{-/-}$ microglia show a reduced upregulation of genes responsible for cell adhesion as compared to WT microglia which underlines the morphological differences upon stimulation. Also, the downregulation of the GO term "negative regulation of cell projection organization" in CB2$^{-/-}$ microglia underlines the differential ramification potential. The lack of morphological changes further supports our previous findings showing a dampened pro-inflammatory response on the gene expression level as well as a decreased secretion of pro-inflammatory mediators (Schmöle, Lundt, Ternes, et al., 2015). This confirms our idea that the CB2 receptor is indispensable for microglial activation.

We additionally analyzed the TLR-mediated activation of BMDM to investigate if the observed effects mediated by CB2-deletion are specific to microglia or present in myeloid cells in general. Since microglia originate from the yolk sac whereas BMDM differentiate from hematopoietic stem cells (Ginhoux & Prinz, 2015), differences in cell-specific phenotypes are possible. BMDM from CB2$^{-/-}$ mice show reduced expression of inflammatory cell surface markers as observed before (Schmöle, Lundt, Ternes, et al., 2015) but the release of inflammatory cytokines was only partially altered. These findings suggest that the CB2-mediated differences on TLR-induced activation are, at least partially, conserved in cells from the myeloid lineage.

FIGURE 5 p38 activity in WT and CB2$^{-/-}$ primary microglia after TLR stimulation. Experimental setup (a). Heatmap of the genes from the KEGG term "MAPK signaling pathway" with the mean expression for each condition scaled by rows (b), gene expression analysis of p38 MAPK encoding genes mapk11 (c) and mapk14 (d) after 16 h stimulation. Treatment effects and genotype effects were observed for mapk11 expression (treatment effect, $F_{3,19} = 7.857$, $p < .01$; genotype effect, $F_{1,19} = 40.18$, $p < .001$) (c) and a genotype effect for mapk14 expression (genotype effect, $F_{1,19} = 29.76$ $p < .001$) (d). Experimental setup of phosphorylation measurement (d). Representative Western Blots (WES System) of p38, pp38 and b-Actin after 16 h stimulation with LPS/IFN-γ, CpG and PolyI:C (e). Analysis of p38 phosphorylation after 30 min revealed a treatment effect and genotype effect (treatment effect, $F_{3,21} = 4.781$, $p < .001$; genotype effect, $F_{1,21} = 12.4$, $p < .001$) (f) and a treatment effect and genotype effect after 16 h of TLR stimulation (treatment effect, $F_{3,25} = 14.15$, $p < .001$; genotype effect, $F_{1,25} = 55.9$, $p < .001$) (g). Data displayed as mean ± SEM. Two-way ANOVA followed by Bonferroni's multiple comparisons. #$p < .05$, ##$p < .01$, ###$p < .001$, *significance to corresponding genotype control. Parts of this figure were created with Biorender

Furthermore, this leads to the idea that infiltrating monocytes from the periphery could also contribute to a reduced inflammatory phenotype since CB2 deletion would reduce peripheral cell recruitment and these cells would be also less activated. This is supported by our previous results showing indeed that CB2 deletion in an AD mouse model led to a reduced infiltration of peripheral macrophages and that these macrophages express less inflammatory cell surface markers (Schmöle, Lundt, Ternes, et al., 2015).

Finally, we aimed at deciphering the molecular mechanisms by which CB2 deletion influences TLR-mediated microglial activation. Up to date, CB2 downstream signaling was reported to include the MAPK/PI3K/ERK and JAK/STAT pathway. CB2 activation induces AKT and ERK1/2 phosphorylation (Bouaboula et al., 1996; Montecucco & Burger, 2008) but suppresses phosphorylation of JAK1/2 and STAT1 (Ehrhart et al., 2005). Our co-expression analysis showed pronounced differences between WT and CB2$^{-/-}$ microglia in the KEGG terms "PI3K-Akt signaling pathway" and "MAPK signaling pathway". We confirmed these findings by demonstrating that stimulation of WT microglia with ligands for TLR3, 4 and 9 induced p38 phosphorylation, which was diminished in CB2$^{-/-}$ microglia. This connects to previous findings from Romero-Sandoval et al (Romero-Sandoval, Horvath, Landry, & DeLeo, 2009), demonstrating that CB2 activation induces MKP-1 and -3 induction and subsequent ERK1/2 dephosphorylation. However, MKP-1 was also reported to not only dephosphorylate ERK1/2 but also p38 (Zhou, Ling, & Dheen, 2007). In contrast, a study in human leukemia cells showed that CB2 activation leads to p38 MAPK activation (Herrera, Carracedo, Diez-Zaera, Guzmán, & Velasco, 2005). These data indicate that CB2 downstream signaling might also include p38 MAPK signaling but the reported discrepancies might be due to the ontogeny of cells from central i.d. yolk-sac or peripheral i.d. hematopoietic origin. Here, for the first time we showed that this pathway is also crucial for microglia CB2-signaling. It is well known that p38 MAPK activation by LPS upregulates the production of inflammatory cytokines such as TNFα and IL6 (Falcicchia, Tozzi, Arancio, Watterson, & Origlia, 2020). This strongly supports our idea that CB2 regulates TLR-induced microglial activity via p38 since we observed diminished p38 phosphorylation in line with a previous report showing decrease in IL-6 and TNFα release (Schmöle, Lundt, Ternes, et al., 2015).

This study highlights MAPK signaling via p38 phosphorylation as a connecting link between dampened TLR-induced microglial activation and CB2 deletion in microglia. Future studies will have to identify the exact mediator of CB2-dependent p38 phosphorylation.

Our findings clearly show a decreased inflammatory response of microglia from CB2$^{-/-}$ mice compared to WT microglia upon stimulation with pro-inflammatory mediators. This further confirms in vitro and in vivo models of microglia from CB2$^{-/-}$ mice that presented a reduced pro-inflammatory phenotype in the response to an inflammatory stimulus such as LPS/IFN-γ or dampened neuroinflammation in an AD mouse model (Schmöle et al., 2018; Schmöle, Lundt, Ternes, et al., 2015). On the other hand, CB2 activation is described to attenuate microglial activation upon pro-inflammatory stimulation (Ma et al., 2015; Merighi et al., 2012; Molina-Holgado et al., 2003),

suggesting an enhanced microglial activation in the absence of CB2. This raises the question if there are differences in acute CB2 activation in pharmacological models as compared to CB2 deletion, which reflects a chronic inactivation of the signaling cascade. Furthermore, up to now, no study exists that investigates potential effects of TLR stimulation on the synthesis of endogenous CB2 ligands, namely 2-AG or anandamide, which in turn could modulate CB2 activity in microglia. Therefore, we cannot exclude that differences between pharmacological and genetic studies on CB2 activity might be indirect effects based on a modulation of the endocannabinoid production.

The role of the CB2 receptor in microglial activation is critical in the case of acute and chronic inflammation. Its expression is downregulated in microglia under acute inflammatory conditions (Carlisle, Marciano-Cabral, Staab, Ludwick, & Cabral, 2002; Mecha et al., 2015; Schmöle, Lundt, Ternes, et al., 2015) but upregulated in the context of several chronic neuroinflammatory diseases (Benito et al., 2008). These findings promoted the idea that the CB2 receptor is crucial to control microglial activation and that its upregulation is necessary to switch microglia from a pro- to anti-inflammatory state to avoid neurotoxic damage (Komorowska-Müller & Schmöle, 2021). Our results from a knock-out model now promote the idea that CB2 is not only needed for the switch, but also for a full activation. This suggests an even more important role for the CB2 receptor in microglia activation than previously thought. However, we are aware that we cannot fully exclude developmental effects of CB2 deletion which have not been investigated so far. Therefore, future studies need to include cell type-specific models and compare constitutive to inducible knock-out models.

Taken together, we demonstrate that the presence of the CB2 receptor is necessary to induce a full TLR-mediated microglial activation, which is mainly mediated by p38 MAPK signaling. Our data strongly supports a crucial role of CB2 for microglia activation and an interference of CB2 receptor signaling with TLR signaling.

CONFLICT OF INTEREST
The authors declare no conflicts of interest.

AUTHOR CONTRIBUTIONS
Marc Beyer, Andreas Zimmer, and Anne-Caroline Schmöle conceived the study; Kishore Aravind Ravichandran, Bolanle Fatimat Olabiyi,

ORCID

Nico Reusch https://orcid.org/0000-0001-5625-0701
Kishore Aravind Ravichandran https://orcid.org/0000-0002-2429-5988
Bolanle Fatimat Olabiyi https://orcid.org/0000-0001-5753-5143
Joanna Agnieszka Komorowska-Müller https://orcid.org/0000-0002-9063-2495
Jan N. Hansen https://orcid.org/0000-0002-0489-7535
Thomas Ulas https://orcid.org/0000-0002-9785-4197
Marc Beyer https://orcid.org/0000-0001-9704-148X
Andreas Zimmer https://orcid.org/0000-0001-6618-6264
Anne-Caroline Schmöle https://orcid.org/0000-0001-7091-6354

REFERENCES

Akira, S., & Takeda, K. (2004). Toll-like receptor signalling. *Nature Reviews Immunology*, 4(7), 499–511. https://doi.org/10.1038/nri1391

Arganda-Carreras, I., Fernández-González, R., Muñoz-Barrutia, A., & Ortiz-De-Solorzano, C. (2010). 3D reconstruction of histological sections: Application to mammary gland tissue. *Microscopy Research and Technique*, 73(11), 1019–1029. https://doi.org/10.1002/jemt.20829

Benito, C., Tolón, R. M., Pazos, M. R., Núñez, E., Castillo, A. I., & Romero, J. (2008). Cannabinoid CB 2 receptors in human brain inflammation. *British Journal of Pharmacology*, 153(2), 277–285. https://doi.org/10.1038/sj.bjp.0707505

Berdyshev, E., Boichot, E., Corbel, M., Germain, N., & Lagente, V. (2002). Effects of cannabinoid receptor ligands on LPS-induced pulmonary inflammation in mice. *Life Sciences*, 63, 125–129. https://doi.org/10.1016/s0024-3205(98)00324-5

Blake, J. A., Christie, K. R., Dolan, M. E., Drabkin, H. J., Hill, D. P., Ni, L., & Westerfeld, M. (2015). Gene ontology consortium: Going forward. *Nucleic Acids Research*, 43(1), 1049–1056. https://doi.org/10.1093/nar/gku1179

Bouaboula, M., Poinot-Chazel, C., Marchand, J., Canat, X., Bourrié, B., Rinaldi-Carmona, M., & Casellas, P. (1996). Signaling pathway associated with stimulation of CB2 peripheral cannabinoid receptor: Involvement of both mitogen-activated protein kinase and induction of Krox-24 expression. *European Journal of Biochemistry*, 237, 704–711. https://doi.org/10.1111/j.1432-1033.1996.0704p.x

Bray, N. L., Pimentel, H., Melsted, P., & Pachter, L. (2016). Near-optimal probabilistic RNA-seq quantification. *Nature Biotechnology*, 34(5), 525–527. https://doi.org/10.1038/nbt.3519

Buckley, N. E., McCoy, K. L., Mezey, É., Bonner, T., Zimmer, A., Felder, C. C., Glass, M., & Zimmer, A. (2000). Immunomodulation by cannabinoids is absent in mice deficient for the cannabinoid CB2receptor. *European Journal of Pharmacology*, 396(2–3), 141–149. https://doi.org/10.1016/S0014-2999(00)00211-9

Carlisle, S. J., Marciano-Cabral, F., Staab, A., Ludwick, C., & Cabral, G. A. (2002). Differential expression of the CB2 cannabinoid receptor by rodent macrophages and macrophage-like cells in relation to cell activation. *International Immunopharmacology*, 2(1), 69–82. https://doi.org/10.1016/S1567-5769(01)00147-3

Concannon, R. M., Okine, B. N., Finn, D. P., & Dowd, E. (2015). Differential upregulation of the cannabinoid CB$_2$ receptor in neurotoxic and inflammation-driven rat models of Parkinson's disease. *Experimental Neurology*, 269, 133–141. https://doi.org/10.1016/j.expneurol.2015.04.007

Downer, E. J., Clifford, E., Gran, B., Nel, H. J., Fallon, P. G., & Moynagh, P. N. (2011). Identification of the synthetic cannabinoid R(+)WIN55,212-2 as a novel regulator of IFN regulatory factor 3 activation and IFN-β expression: Relevance to therapeutic effects in models of multiple sclerosis. *Journal of Biological Chemistry*, 286(12), 316–328. https://doi.org/10.1074/jbc.M110.188599

Ehrhart, J., Obregon, D., Mori, T., Hou, H., Sun, N., Bai, Y., Klein, T., Fernandez, F., Tan, J., & Shytle, D. (2005). Stimulation of cannabinoid receptor 2 (CB2) suppresses microglial activation. *Journal of Neuroinflammation*, 2, 1–13. https://doi.org/10.1186/1742-2094-2-29

Fabregat, A., Sidiropoulos, K., Garapati, P., Gillespie, M., Hausmann, K., Haw, R., Jassal, B., Jupe, S., Korninger, F., McKay, S., Matthews, L., May, B., Milacic, M., Rothfels, K., Shamovsky, V., Webber, M., Weiser, J., Williams, M., Wu, G., ... D'Eustachio, P. (2016). The reactome pathway knowledgebase. *Nucleic Acids Research*, 44(1), 481–487. https://doi.org/10.1093/nar/gkv1351

Falcicchia, C., Tozzi, F., Arancio, O., Watterson, D. M., & Origlia, N. (2020). Involvement of p38 mapk in synaptic function and dysfunction. *International Journal of Molecular Sciences*, 21(16), 1–14. https://doi.org/10.3390/ijms21165624

Fiebich, B. L., Batista, C. R. A., Saliba, S. W., Yousif, N. M., & de Oliveira, A. C. P. (2018). Role of microglia TLRs in neurodegeneration. *Frontiers in Cellular Neuroscience*, 12, 329. https://doi.org/10.3389/fncel.2018.00329

Flannery, L. E., Henry, R. J., Kerr, D. M., Finn, D. P., & Roche, M. (2018). FAAH, but not MAGL, inhibition modulates acute TLR3-induced neuroimmune signaling in the rat, independent of sex. *Journal of Neuroscience Research*, 96(6), 989–1001. https://doi.org/10.1002/jnr.24120

Fulton, D. L., Sundararajan, S., Badis, G., Hughes, T. R., Wasserman, W. W., Roach, J. C., & Sladek, R. (2009). TFCat: The curated catalog of mouse and human transcription factors. *Genome Biology*, 10(3), 29.

Gallily, R., Yamin, A., Waksmann, Y., Ovadia, H., Weidenfeld, J., Bar-Joseph, A., & Shohami, E. (1997). Protection against septic shock and suppression of tumor necrosis factor alpha and nitric oxide production by dexanabinol (HU-211), a nonpsychotropic cannabinoid. *The Journal of Pharmacology and Experimental Therapeutics*, 283(2), 918–924.

Ginhoux, F., & Prinz, M. (2015). Origin of microglia: Current concepts and past controversies. *Cold Spring Harbor Perspectives in Biology*, 7(8), 1–15. https://doi.org/10.1101/cshperspect.a020537

Henry, R. J., Kerr, D. M., Finn, D. P., & Roche, M. (2014). FAAH-mediated modulation of TLR3-induced neuroinflammation in the rat hippocampus. *Journal of Neuroimmunology*, 276(1–2), 126–134. https://doi.org/10.1016/j.jneuroim.2014.09.002

Herrera, B., Carracedo, A., Diez-Zaera, M., Guzmán, M., & Velasco, G. (2005). p38 MAPK is involved in CB2 receptor-induced apoptosis of human leukaemia cells. *FEBS Letters*, 579(22), 5084–5088. https://doi.org/10.1016/j.febslet.2005.08.021

Ibsen, M. S., Connor, M., & Glass, M. (2017). Cannabinoid CB 1 and CB 2 receptor signaling and bias. *Cannabis and Cannabinoid Research*, 2(1), 48–60. https://doi.org/10.1089/can.2016.0037

Kanehisa, M. (2000). KEGG: Kyoto encyclopedia of genes and genomes. *Nucleic Acids Research*, 28(1), 27–30. https://doi.org/10.1093/nar/28.1.27

Kawasaki, T., & Kawai, T. (2014). Toll-like receptor signaling pathways. *Frontiers in Immunology*, 5(5625), 1524–1525. https://doi.org/10.3389/fimmu.2014.00461

Keenan, A. B., Torre, D., Lachmann, A., Leong, A. K., Wojciechowicz, M. L., Utti, V., & Ma'ayan, A. (2019). ChEA3: Transcription factor enrichment analysis by orthogonal omics integration. *Nucleic Acids Research*, 47(1), 212–224. https://doi.org/10.1093/nar/gkz446

Kielian, T. (2006). Toll-like receptors in central nervous system glial inflammation and homeostasis. *Journal of Neuroscience Research*, 83(5), 711–730. https://doi.org/10.1002/jnr.20767

Kim, C., Cho, E. D., Kim, H. K., You, S., Lee, H. J., Hwang, D., & Lee, S. J. (2014). Β1-integrin-dependent migration of microglia in response to neuron-released Α-synuclein. *Experimental and Molecular Medicine*, 46(4), 1–10. https://doi.org/10.1038/emm.2014.6

Komorowska-Müller, J. A., & Schmöle, A. C. (2021). CB2 receptor in microglia: The guardian of self-control. *International Journal of Molecular Sciences*, 22(1), 1–27. https://doi.org/10.3390/ijms22010019

Liberzon, A., Birger, C., Thorvaldsdóttir, H., Ghandi, M., Mesirov, J. P., & Tamayo, P. (2015). The molecular signatures database hallmark gene set collection. *Cell Systems*, 1(6), 417–425. https://doi.org/10.1016/j.cels.2015.12.004

Love, M. I., Huber, W., & Anders, S. (2014). Moderated estimation of fold change and dispersion for RNA-seq data with DESeq2. *Genome Biology*, 15(12), 1–21. https://doi.org/10.1186/s13059-014-0550-8

Ma, L., Jia, J., Liu, X., Bai, F., Wang, Q., & Xiong, L. (2015). Activation of murine microglial N9 cells is attenuated through cannabinoid receptor CB2 signaling. *Biochemical and Biophysical Research Communications*, 458(1), 92–97. https://doi.org/10.1016/j.bbrc.2015.01.073

Maresz, K., Carrier, E. J., Ponomarev, E. D., Hillard, C. J., & Dittel, B. N. (2005). Modulation of the cannabinoid CB2 receptor in microglial cells in response to inflammatory stimuli. *Journal of Neurochemistry*, 95(2), 437–445. https://doi.org/10.1111/j.1471-4159.2005.03380.x

Mecha, M., Feliú, A., Carrillo-Salinas, F. J., Rueda-Zubiaurre, A., Ortega-Gutiérrez, S., de Sola, R. G., & Guaza, C. (2015). Endocannabinoids drive the acquisition of an alternative phenotype in microglia. *Brain, Behavior, and Immunity*, 49, 233–245. https://doi.org/10.1016/j.bbi.2015.06.002

Merighi, S., Gessi, S., Varani, K., Simioni, C., Fazzi, D., Mirandola, P., & Borea, P. A. (2012). Cannabinoid CB2 receptors modulate ERK-1/2 kinase signalling and NO release in microglial cells stimulated with bacterial lipopolysaccharide. *British Journal of Pharmacology*, 165(6), 1773–1788. https://doi.org/10.1111/j.1476-5381.2011.01673.x

Mestre, L., Correa, F., Arévalo-Martín, A., Molina-Holgado, E., Valenti, M., Ortar, G., di Marzo, V., & Guaza, C. (2005). Pharmacological modulation of the endocannabinoid system in a viral model of multiple sclerosis. *Journal of Neurochemistry*, 92, 1327–1339. https://doi.org/10.1111/j.1471-4159.2004.02979.x

Milner, R., & Campbell, I. L. (2003). The extracellular matrix and cytokines regulate microglial integrin expression and activation. *The Journal of Immunology*, 170(7), 3850–3858. https://doi.org/10.4049/jimmunol.170.7.3850

Molina-Holgado, F., Pinteaux, E., Moore, J. D., Molina-Holgado, E., Guaza, C., Gibson, R. M., & Rothwell, N. J. (2003). Endogenous Interleukin-1 receptor antagonist mediates anti-inflammatory and neuroprotective actions of cannabinoids in neurons and glia. *The Journal of Neuroscience*, 23, 6470–6474. https://doi.org/10.1523/jneurosci.23-16-06470.2003

Montecucco, F., & Burger, F. (2008). CB 2 cannabinoid receptor agonist JWH-015 modulates human monocyte migration through defined intracellular signaling pathways. *American Journal of Physiology. Heart and Circulatory Physiology*, 294, 1145–1155. https://doi.org/10.1152/ajpheart.01328.2007

Mukhopadhyay, S., Das, S., Williams, E. A., Moore, D., Jones, J. D., Zahm, D. S., Ndengele, M. M., Lechner, A. J., & Howlett, A. C. (2006). Lipopolysaccharide and cyclic AMP regulation of CB 2 cannabinoid receptor levels in rat brain and mouse RAW 264.7 macrophages. *Journal of Neuroimmunology*, 181, 82–92. https://doi.org/10.1016/j.jneuroim.2006.08.002

Pacher, P., & Mechoulam, R. (2011). Is lipid signaling through cannabinoid 2 receptors part of a protective system? *Progress in Lipid Research*, 50, 193–211. https://doi.org/10.1016/j.plipres.2011.01.001

Plescher, M., Seifert, G., Hansen, J. N., Bedner, P., Steinhäuser, C., & Halle, A. (2018). Plaque-dependent morphological and electrophysiological heterogeneity of microglia in an Alzheimer's disease mouse model. *GLIA*, 66, 1464–1480. https://doi.org/10.1002/glia.23318

Ritchie, M. E., Phipson, B., Wu, D., Hu, Y., Law, C. W., Shi, W., & Smyth, G. K. (2015). Limma powers differential expression analyses for RNA-sequencing and microarray studies. *Nucleic Acids Research*, 43(7), e47. https://doi.org/10.1093/nar/gkv007

Roche, M., Diamond, M., Kelly, J. P., & Finn, D. P. (2006). In vivo modulation of LPS-induced alterations in brain and peripheral cytokines and HPA axis activity by cannabinoids. *Journal of Neuroimmunology*, 181, 57–67. https://doi.org/10.1016/j.jneuroim.2006.08.001

Romero-Sandoval, E. A., Horvath, R., Landry, R. P., & DeLeo, J. A. (2009). Cannabinoid receptor type 2 activation induces a microglial anti-inflammatory phenotype and reduces migration via MKP induction and ERK dephosphorylation. *Molecular Pain*, 5, 1–15. https://doi.org/10.1186/1744-8069-5-25

Schmöle, A., Lundt, R., Ternes, S., Albayram, Ö., Ulas, T., Schultze, J. L., & Zimmer, A. (2015). Cannabinoid receptor 2 deficiency results in reduced neuroinflammation in an Alzheimer's disease mouse model. *Neurobiology of Aging*, 36(2), 710–719. https://doi.org/10.1016/j.neurobiolaging.2014.09.019

Schmöle, A., Lundt, R., Toporowski, G., Hansen, J. N., Beins, E., Halle, A., & Zimmer, A. (2018). Cannabinoid receptor 2-deficiency ameliorates disease symptoms in a mouse model with Alzheimer's disease-like pathology. *Journal of Alzheimer's Disease*, 64(2), 379–392. https://doi.org/10.3233/JAD-180230

Schmöle, A. C., Lundt, R., Gennequin, B., Schrage, H., Beins, E., Krämer, A., Zimmer, T., Limmer, A., Zimmer, A., & Otte, D. M. (2015). Expression analysis of CB2-GFP BAC transgenic mice. *PLoS One*, 10(9), 1–16. https://doi.org/10.1371/journal.pone.0138986

Shaftel, S. S., Carlson, T. J., Olschowka, J. A., Kyrkanides, S., Matousek, S. B., & O'Banion, M. K. (2007). Chronic interleukin-1β expression in mouse brain leads to leukocyte infiltration and neutrophil-independent blood-brain barrier permeability without overt neurodegeneration. *Journal of Neuroscience*, 27(35), 9301–9309. https://doi.org/10.1523/JNEUROSCI.1418-07.2007

Smith, S. R., Terminelli, C., & Denhardt, G. (2000). Effects of cannabinoid receptor agonist and antagonist ligands on production of inflammatory cytokines and anti-inflammatory interleukin-10 in endotoxemic mice. *The Journal of Pharmacology and Experimental Therapeutics*, 293(1), 136–150.

Soneson, C., Love, M. I., & Robinson, M. D. (2015). Differential analyses for RNA-seq: Transcript-level estimates improve gene-level inferences. *F1000Research*, 4, 1521. https://doi.org/10.12688/f1000research.7563.1

Stempel, A. V., Stumpf, A., Zhang, H. Y., ??zdo??an, T., Pannasch, U., Theis, A. K., & Schmitz, D. (2014). Cannabinoid type 2 receptors mediate a cell type-specific plasticity in the hippocampus. *Neuron*, 90, 795–809. https://doi.org/10.1016/j.neuron.2016.03.034

Tanaka, M., Sackett, S., & Zhang, Y. (2020). Endocannabinoid modulation of microglial phenotypes in neuropathology. *Frontiers in Neurology*, 11, 87. https://doi.org/10.3389/fneur.2020.00087

Tschöp, J., Kasten, K. R., Nogueiras, R., Goetzman, H. S., Cave, C. M., England, L. G., Dattilo, J., Lentsch, A. B., Tschöp, M. H., & Caldwell, C. C. (2009). The cannabinoid receptor 2 is critical for the

host response to sepsis. *The Journal of Immunology.*, *183*, 499–505. https://doi.org/10.4049/jimmunol.0900203

Uhlén, M., Fagerberg, L., Hallström, B. M., Lindskog, C., Oksvold, P., Mardinoglu, A., & Pontén, F. (2015). Tissue-based map of the human proteome. *Science*, *347*(20), 419.

Wolf, S. A., Boddeke, H. W. G. M., & Kettenmann, H. (2017). Microglia in physiology and disease. *Annual Review of Physiology*, *79*, 619–643. https://doi.org/10.1146/annurev-physiol-022516-034406

Yousef, H., Czupalla, C. J., Lee, D., Chen, M. B., Burke, A. N., Zera, K. A., Zandstra, J., Berber, E., Lehallier, B., Mathur, V., Nair, R. V., Bonanno, L. N., Yang, A. C., Peterson, T., Hadeiba, H., Merkel, T., Körbelin, J., Schwaninger, M., Buckwalter, M. S., … Wyss-Coray, T. (2019). Aged blood impairs hippocampal neural precursor activity and activates microglia via brain endothelial cell VCAM1. *Nature Medicine*, *25*(6), 988–1000. https://doi.org/10.1038/s41591-019-0440-4

Yousif, N. M., de Oliveira, A. C. P., Brioschi, S., Huell, M., Biber, K., & Fiebich, B. L. (2018). Activation of EP2 receptor suppresses poly(I: C) and LPS-mediated inflammation in primary microglia and organotypic hippocampal slice cultures: Contributing role for MAPKs. *GLIA*, *66*, 708–724. https://doi.org/10.1002/glia.23276

Zheng, Z. M., & Specter, S. C. (1996). Delta-9-tetrahydrocannabinol suppresses tumor necrosis factor α maturation and secretion but not its transcription in mouse macrophages. *International Journal of Immunopharmacology*, *18*, 53–68. https://doi.org/10.1016/0192-0561(95)00107-7

Zhou, Y., Ling, E. A., & Dheen, S. T. (2007). Dexamethasone suppresses monocyte chemoattractant protein-1 production via mitogen activated protein kinase phosphatase-1 dependent inhibition of Jun N-terminal kinase and p38 mitogen-activated protein kinase in activated rat microglia. *Journal of Neurochemistry*, *102*(3), 667–678. https://doi.org/10.1111/j.1471-4159.2007.04535.x

Zurier, R. B., Rossetti, R. G., Burstein, S. H., & Bidinger, B. (2003). Suppression of human monocyte interleukin-1β production by ajulemic acid, a nonpsychoactive cannabinoid. *Biochemical Pharmacology*, *65*, 649–655. https://doi.org/10.1016/S0006-2952(02)01604-0

SUPPORTING INFORMATION

Additional supporting information may be found in the online version of the article at the publisher's website.